

Morphology-Preserved Alloying in Anisotropic Gold Nanoparticles Using Atomically Precise Nanoclusters

Amrita Chakraborty, Sujan Manna, Biswajit Mondal, Mohammad Bodiuzzaman, Ankit Nagar, Soham Chowdhury, Tanmayaa Nayak, Nonappa, and Thalappil Pradeep*

Noble metal nanoparticles (NPs) exhibit superior plasmonic, catalytic, electronic, and magnetic properties upon alloying with a second metal. However, the synthesis of bimetallic alloy NPs of non-spherical morphologies presents a challenge due to the necessity of concurrently modulating the nucleation and growth kinetics of various metallic constituents. In this study, a simple solution-phase reaction between a phosphine-protected copper nanocluster (NC), namely $[\text{Cu}_{18}(\text{DPPE})_6\text{H}_{16}]^{2+}$ [DPPE = 1,2-bis(diphenyl phosphino)ethane] (abbreviated as Cu_{18}) and gold nanotriangles (AuNTs) is reported as a straightforward strategy to obtain gold-copper alloy nanotriangles (AuCuNTs) while keeping their sizes and sharp edges intact. Extending this protocol to gold nanorods (AuNRs) and nanocubes (AuNCBs) demonstrates its generality for creating anisotropic AuCu alloy NPs. Auger spectroscopic analyses confirm that Cu(0) is the predominant Cu species in the AuCuNTs, indicating that oxidation of Cu in the resulting nanostructures is prevented. A further interaction of AuCuNTs with $[\text{Ag}_{25}(\text{DMBT})_{18}]^-$ [DMBT = 2,4-dimethylbenzenethiol] (abbreviated as Ag_{25}) has yielded AuCuAgNTs, offering a facile synthetic route to trimetallic anisotropic NPs. Thus, the current study corroborates atomically precise metal NCs as versatile precursors for tuning the composition of plasmonic anisotropic NPs to meet diverse technological and industrial needs.

synergetic interaction between different metals, bi- and trimetallic nanostructures have shown remarkably improved physicochemical properties, making them attractive nanoprobes in Surface-enhanced Raman spectroscopy (SERS)-based sensing,^[4] catalysis,^[5,6] photothermal therapy,^[7] and solar cells.^[8] Depending on the reaction mechanism, different metals can combine to form diverse morphologies ranging from crown-jewel, hollow, heterostructure, core-shell, alloyed, and nanosnowmen to porous structures.^[9–13] Among noble metals, Au and Cu possess common face-centered cubic (fcc) crystal structures and share similar valences (+1). Moreover, the relatively minor difference in atomic radii (less than 15%) and the modest discrepancy in molar heat of vaporization (merely 11%) between Au and Cu suggests a strong propensity for nanoscale mixing that facilitates the synthesis of Au–Cu alloy nanostructures. Such Au–Cu alloy NPs serve as cost-effective candidates while showing superior catalytic activity, compared to pure Au NPs.^[14] More recently, Au_3Cu tetrapod nanocrystals (TPNCs) have shown excellent

photothermal performance,^[15] while hollow Au–Cu alloy rods exhibited enhanced catalytic activity compared to the solid alloy nanorods and spherical NPs.^[16] Highly branched Au–Cu nanostructures have been used for non-enzymatic specific detection of glucose and hydrogen peroxide.^[17] These results indicate the relative distribution of different planes, edges, and corners, which makes the non-spherical NPs show optimal performances.^[18] Despite the recent advances yielding bimetallic NPs with dilute concentrations of a secondary metal in low-index, and high-index surface facets,^[19] the synthesis of anisotropic homogeneous alloy NPs faced great challenges. Different metals often require distinct thermodynamic or kinetic conditions for deposition,^[13] making it difficult to achieve precise control over reaction parameters to guide the growth along specific crystallographic directions. Solution phase synthesis of Au–Cu alloy nanocubes,^[20] nanorods,^[21] nanopentacles,^[7] and nanotriangles^[22] either necessitated elevated temperatures, use of lasers, or specialized organic solvents, often yielding success specific to a particular shape. Thus, the independent control over both morphology and composition of anisotropic Au–Cu nanostructures is still an unmet need. Considering the availability of diverse shapes of AuNPs

1. Introduction

Noble metal nanoparticles (NPs) exhibit unique optical properties that are sensitive to their dimensions, morphologies, compositions, and dielectric environments.^[1–3] Due to

A. Chakraborty, S. Manna, B. Mondal, M. Bodiuzzaman, A. Nagar, S. Chowdhury, T. Nayak, T. Pradeep
Department of Chemistry
DST Unit of Nanoscience (DST UNS) and Thematic Unit of Excellence (TUE)
Indian Institute of Technology Madras
Chennai 600 036, India
E-mail: pradeep@iitm.ac.in
Nonappa
Faculty of Engineering and Natural Sciences
Tampere University
Tampere FI-33720, Finland

The ORCID identification number(s) for the author(s) of this article can be found under <https://doi.org/10.1002/sml.202410784>

DOI: 10.1002/sml.202410784

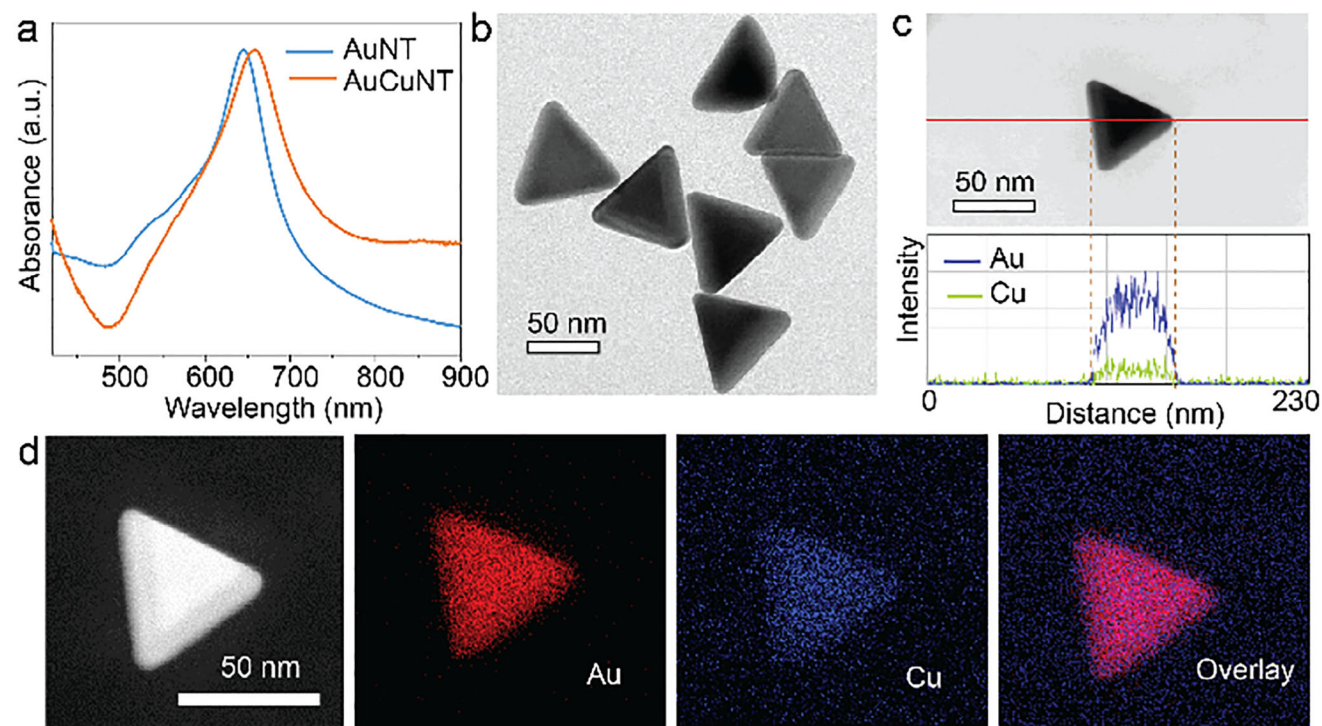


Figure 1. Characterization of AuCuNTs. a) Absorption spectra of parent AuNT and alloy AuCuNTs. b) TEM image of AuCuNTs showing size and shape uniformity. c) Bright-field STEM EDS line profile and d) dark-field STEM image of a single AuCuNT along with corresponding EDS elemental mapping that shows uniform distribution of Au and Cu along the NTs.

in the literature, we envisioned a strategy of doping elemental Cu to these AuNPs, keeping their morphology unaltered as a generic route to synthesize Au–Cu alloy anisotropic NPs of desired morphology and composition. For this, we chose planar gold nanotriangles (AuNTs) as a model anisotropic NP as their sharp edges are highly sensitive toward any morphological changes during the alloy formation. The approach developed has been extended to gold nanorods (AuNRs) and gold nanocubes (AuNCBs).

Since their discovery in the 1960s, atomically precise noble metal nanoclusters (NCs) have garnered significant interest due to their distinctive molecule-like optoelectronic properties,^[23,24] as well as their catalytic activities,^[25] among other applications. They form colloidal assemblies with anisotropic NPs such as tellurium nanowires,^[26] and AuNRs,^[27] leading to novel composite materials. Recently, spontaneous solution phase reaction has emerged as a facile route towards doping heteroatom into ultra-small NCs^[28] as well as plasmonic NPs.^[29,30] Inspired by these results, we studied the chemical reactivity of $[\text{Cu}_{18}(\text{DPPE})_6\text{H}_{16}]^{2+}$ where DPPE = 1,2-bis(diphenylphosphino)ethane (abbreviated herein as Cu_{18}), with AuNTs to demonstrate a unique strategy of alloy formation without altering the morphology of the latter. This approach has been extended to AuNRs and AuNCBs that yielded gold-copper alloy nanorods (AuCuNRs) and alloy nanocubes (AuCuNCBs), respectively, with high size and shape monodispersity. We further extended the protocol to silver NCs to make trimetallic gold-copper-silver (AuCuAg) nanostructures.

2. Results and Discussion

The synthesis of Cu_{18} NC was adapted from the methodology established by Li et al.^[31] The emergence of an orange color in the solution and the characteristic UV–vis absorption spectrum suggested the successful formation of Cu_{18} NC, which was further confirmed by the two peaks at m/z 3552 and 1775 in electrospray ionization mass spectrum (ESI MS) (Figure S1, Supporting Information). As a monometallic template, planar AuNTs of ≈ 75.5 nm edge-length were synthesized via a seed-mediated growth protocol reported by Scarabelli et al.^[32] As illustrated in Figure S2 (Supporting Information), the purified AuNTs exhibited a high degree of uniformity in size and shape. These AuNTs were dispersed in *N,N*-Dimethylformamide (DMF), to which, Cu_{18} NC was added under moderate stirring at room temperature. UV–vis absorption spectra of the particles, before and after the reaction, are presented in Figure 1a, where the resultant AuCuNTs exhibit a red shift in the localized surface plasmon resonance (LSPR) peak position. Alloying of Cu into Au NPs is known to cause such a red shift along with a broadening of the LSPR band.^[33] Transmission electron microscopy (TEM) image of the reacted AuNTs, as shown in Figure 1b and Figure S3a (Supporting Information), confirmed preserving the planar triangular morphology post-reaction. Moreover, a comprehensive analysis of the edge-length distribution of the NTs before and after the reaction shows negligible changes in their sizes (Figure S2c, Supporting Information), suggesting that the observed spectral shift in Figure 1a was attributable to the alloying process.

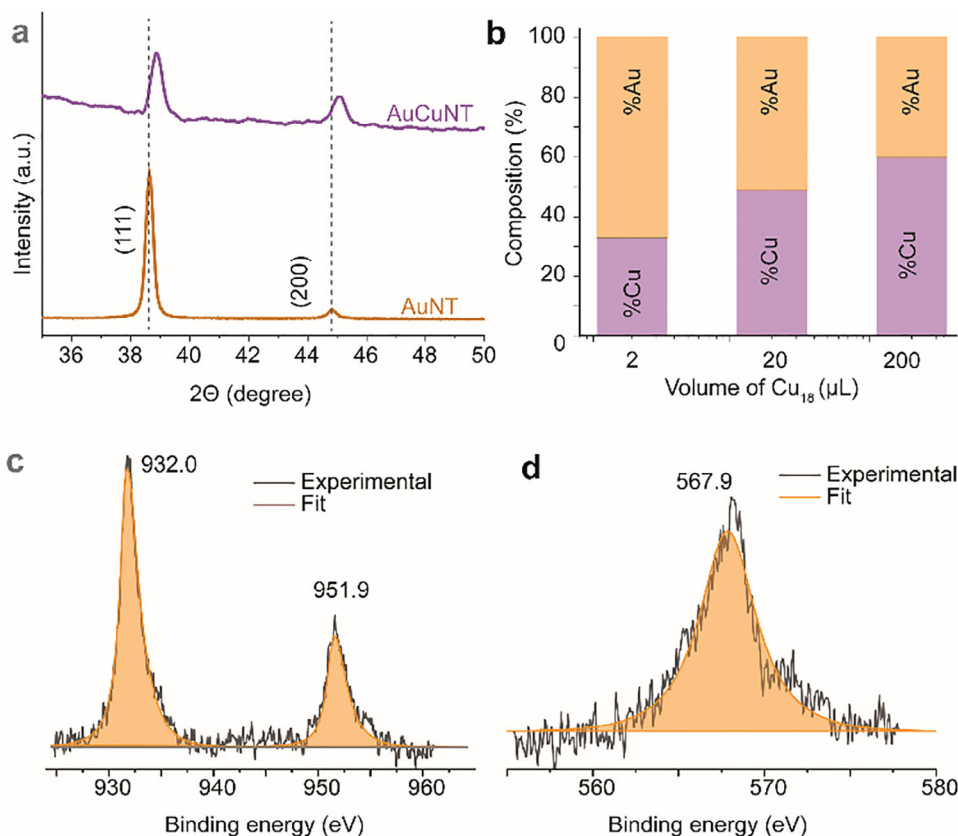


Figure 2. a) Comparative XRD spectra before and after reaction showing increased 2θ , i.e., decreased lattice spacing in AuCuNT, b) Variation of atomic % of Cu and Au in AuCuNTs as a function of Cu₁₈ concentration in the reaction medium, c) Cu 2p X-ray photoelectron spectrum and d) Cu LMM Auger showing the presence of Cu(0) exclusively in AuCuNT.

Scanning transmission electron microscopy (STEM) and corresponding energy-dispersive X-ray spectroscopy (EDS) offer a powerful visual confirmation to distinguish alloy versus core-shell structures.^[34] STEM-EDS line scans show that in homogeneous alloys the two metals are equally distributed throughout each particle, whereas a core-shell particle shows a bimodal elemental distribution with one element enriched in the shell.^[35,36] Bright-field STEM image of an isolated AuCuNT and the corresponding line scan (Figure 1c) demonstrate a homogeneous distribution of Au and Cu along the NTs, which indicates alloy formation. High-angle annular dark-field STEM (HAADF-STEM) and corresponding EDS mapping were also performed on the NTs. As shown in Figure 1d, they further confirm the integration of Au and Cu within the NTs, keeping their sharp edges and flat faces intact. Figure S3b (Supporting Information) presents EDS line scans of three additional AuCuNTs. Comparable intensities for Au and Cu in all of them confirm the uniform composition of AuCuNTs at the single-particle level. We further conducted inductively coupled plasma mass spectrometry (ICP-MS) on both the parent AuNTs and the AuCuNTs. As summarized in Figure S3c (Supporting Information), the ICP-MS results confirm that the AuCuNTs have an Au:Cu ratio of ≈ 5.7 , which matches closely with the ratio observed in the STEM EDS study (Au:Cu = 5.5).

Powder X-ray diffraction (PXRD) is a reliable technique for determining the structure and the crystallinity of metallic NPs. The

comprehensive XRD spectra of AuNTs and AuCuNTs, as depicted in Figure S4 (Supporting Information), show a single-phase face-centered cubic (fcc) pattern. A magnified view of the peaks corresponding to (111) and (200) planes in Figure 2a reveals a discernible shift towards higher 2θ values in AuCuNTs, validating the formation of an Au-Cu alloy.^[33] According to the calibration curve of lattice parameter based on the XRD peak positions proposed by Chang et al.,^[37] lattice parameter of AuNT is calculated to be 4.050 Å, whereas that of AuCuNT is 4.036 Å in our case. This suggests uniform alloying of 88% elemental Au and 12% Cu, over the possibilities of Cu shell formation or surface-limited Cu doping. The observed broadening of XRD peaks in AuCuNTs may be attributed to the uncertainty of composition within the AuCuNTs. Further, the absence of a superlattice peak (110) confirms that the alloy possesses atomic disorder.^[38] This finding speaks for the unique reactivity of Cu₁₈ NC towards AuNTs. Previously, in the case of a similar reaction between AuNTs and [Ag₂₅(DMBT)₁₈]⁻ [DMBT = 2,4-dimethylbenzenethiol] (abbreviated as Ag₂₅), the XRD peak positions reflected no shift. Besides, the concentration of the reactant NC, Ag₂₅, had little effect on the low elemental ratio of Ag to Au in the resulting bimetallic NT, indicating that Ag doping was limited to the surface of the AuNTs.^[29] As a result, the concentration of the reactant NC, Ag₂₅, had little effect on the composition of the resulting bimetallic NTs. However, varying atomic ratio of the metallic components within alloy

NPs often alters their photoluminescent properties,^[39] catalytic efficiency,^[40,41] SERS performance.^[42] Therefore, it is beneficial to have the freedom to tune the composition of the NTs without altering their morphology. In this study, the atomic percentage of Cu in the resulting NTs was modulated simply by varying the concentration of Cu₁₈ NC in the reaction medium. The Cu content within the AuCuNTs, as obtained from their TEM EDS analysis, is graphically represented against the NC concentration in Figure 2b (NTs of the same sample showed ±3% variation in Cu content). The quantitative correlation indicates that the Cu content of the NTs increased up to 60% upon the addition of 200 μL of 1.35 mg mL⁻¹ Cu NC. This observation is consistent with most Au–Cu alloy NPs that exhibit a linear dependency between the alloy's metallic composition and the precursor metal concentration introduced.^[43]

A major challenge faced by Cu and Cu-based NPs is their pronounced vulnerability to oxidation.^[44] Cu colloids tend to turn yellow or precipitate immediately upon exposure to air in solution, forming copper(I) oxide (Cu₂O) or copper(II) oxide (CuO). Incorporating Au into Cu NPs has been a popular approach for protecting Cu NPs from oxidation.^[45] In the case of AuCuNTs, the absence of an additional XRD peak for the (110) plane at 29.60° of Cu₂O indicates the absence of an oxide layer surrounding the NTs.^[46] AuCuNTs were further investigated by performing X-ray photoelectron spectroscopy (XPS) and corresponding Auger transitions. The XPS survey spectrum is presented in Figure S5a (Supporting Information). The atomic composition derived from the spectrum indicates 88% elemental Au and 12% elemental Cu. These values rule out the possibility of the formation of a Cu shell on AuNTs, as such configurations would result in a predominant Cu signal in XPS. For example, Sakthisabarimoorathi et al. observed no detectable Cu signal in the XPS analysis of Cu core-Ag shell particles.^[47] The Au 4f region (Figure S5b, Supporting Information) contained the two characteristic peaks for metallic Au, whereas, Cu 2p region of the XPS spectrum (Figure 2c) indicates the presence of Cu⁰ and/or Cu⁺ from the two distinct peaks at 932.0 eV (Cu 2p_{3/2}) and 951.9 eV (Cu 2p_{1/2}) along with the absence of Cu²⁺ satellite peaks in between them. Since it is difficult to distinguish between Cu⁰ and Cu⁺ from their XPS spectrum, the Cu LMM region of the Auger transition is depicted in Figure 2d. A single peak at 567.9 eV in the binding energy axis, i.e., 918.7 eV in terms of kinetic energy (kinetic energy = 1486.6 eV – 567.9 eV = 918.7 eV), is the characteristic Auger peak of metallic Cu.^[48] Notably, the absence of peaks due to Cu⁺ and Cu²⁺ (916.4 and 917.8 eV, respectively) proves that Cu is incorporated in the alloy NTs solely in its metallic form. In core-shell structures, the shell-forming metal is typically found in its oxidized form.^[49] Here, the presence of Cu exclusively in Cu(0) state further mitigates the possibility of core-shell morphology. Homogeneous Au–Cu alloying in a highly anisotropic nanoparticle without altering its morphological features is a unique finding and warrants further investigation into the overall reaction mechanism.

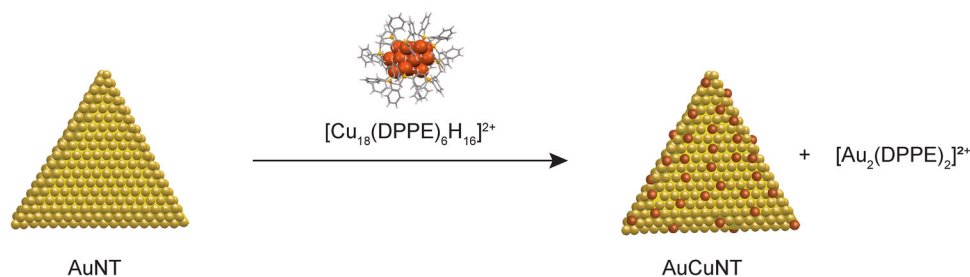
Unlike NP-NC reactions reported so far,^[29] here the size and shape of the reacted NTs remained unaltered, necessitating additional experiments to assess potential Au etching. At various Cu₁₈ concentrations, the reaction mixture was centrifuged to precipitate the AuCuNTs. UV–vis spectroscopy and TEM were employed to confirm the absence of AuNTs in the supernatant prior

to performing the ICP-MS to quantify the Au etched out to the reaction mixture. A control experiment was also conducted in which an equivalent volume of DMF, instead of Cu₁₈, was added to maintain the volume constant. The ICP-MS results from three distinct sets of reactions are compiled in Table S1 (Supporting Information). A significant increase in the quantity of Au atoms leached into the reaction medium was observed with the addition of Cu₁₈. This trend approached saturation at higher NC concentrations. This observation, combined with Figure 2b, indicates that with the course of the reaction, the amount of Cu increased in the NTs, and the amount of Au increased in the supernatant, i.e., some of the Au atoms within the AuNTs were replaced by Cu atoms. Additionally, ESI MS analysis of the same supernatant was performed to identify the charge state of etched Au in the dispersion. The MS depicted in Figure S6 (Supporting Information) confirms the presence of [Au₂(DPPE)₂]²⁺ ions in the dispersion. The isotopic distribution pattern of the experimental peak at m/z 595, as shown in the inset, aligns precisely with the theoretical counterpart, which confirms that Au(0) leaches out in the form of [Au₂(DPPE)₂]²⁺ (Statement 1).

Now, oxidation of Au(0) by Cuⁿ⁺ is not expected when the standard electrode reduction potentials are considered. However, due to the quantum confinement effect, the oxidation potential of metal NPs greatly decreases.^[50] As a result, nanoscopic systems, especially those less than 3 nm in diameter often participate in unconventional redox behavior, where Au NPs are known to be oxidized by less noble metal ions.^[51–53] Such redox reactions, unexpected based on classical galvanic theory, are referred to as “anti-galvanic” reduction (AGR). Studies on noble metal NCs have reported that AGR is dependent on several factors such as surface ligand, ion precursor, ion dosage, solvent, and so on.^[30,53–57] Here, to identify the Cu precursor in the present case, we conducted a control experiment where Cu₁₈ NC was treated in an equivalent reaction condition in absence of AuNTs, and the ESI MS was analyzed. As depicted in Figure S8 (Supporting Information), [Cu_xDPPE_y]⁺ (x = 1, y = 1, 2) complexes were identified. Such Cu-DPPE complexes of varying composition were presumably generated in situ that reacted with the AuNTs (Statement 2).

Ciganda et al. have shown that surface ligands play a crucial role as AuNPs act as electron reservoir redox catalysts.^[58] Precisely, ligand-free and surfactant-free gold NPs are known to reduce Ag and Cu ions as the oxidation potential value of bare AuNPs is sufficiently lower, which presumably is the driving force of AGR.^[53] Here, although the AuNTs purified by flocculation method (“purified AuNTs”) showed characteristic peaks of CTAC in their IR spectrum (Figure S7, Supporting Information), after the removal of excess CTAC by centrifugation (denoted as “clean AuNTs”), no such IR peaks were observed. This can be attributed to the fact that the low propensity of Cl⁻ for the Au surface causes the CTA⁺ micelles to detach from the AuNT leaving a few disordered CTA⁺ ions sticking to the surface, as reported by Meena et al.^[59] Thus, we believe that unprotected Au atoms coexisted on the AuNT surface along with the CTA⁺-protected sites. These bare Au atoms were accessible to any reactant present in the reaction medium and might have acted as the starting points of the AGR reaction (Statement 3).

Here, a complete characterization of the reaction intermediates was not possible, making it difficult to explain the exact reaction mechanism. However, using dispersion correction



Scheme 1. Schematic representation of the fabrication of AuCuNT.

density functional theory, Peng et al. have demonstrated that foreign metal atoms in the form of ML_2 ($\text{M}=\text{Ag}, \text{Cd}, \text{Hg}, \text{L} = \text{thiolate}$) can rapidly diffuse to the surface of Au_{25} NC. Later, it can slowly diffuse to the icosahedral core of the NC releasing AuL_2 moieties.^[60] We believe that a similar mechanism takes place in the present case where $\text{L} = \text{DPPE}$ and $\text{M}=\text{Cu}$. Here, Cu is first incorporated into the AuNT surface, and later relocated towards the interior, as observed in many AuCu alloy NPs.^[61,62] Molecular rearrangements of metal-phosphine complexes on Au NC surface observed by Wang et al. align well with our hypothesis.^[63] Au has a larger atomic radius, and such elemental distribution reduces the total number of surface atoms, thereby decreasing the surface energy associated with broken bonds at the surface. Using decahedrons, Guisbiers et al. have shown that at room temperature, the formation energy of a Cu core- Au shell NP is comparable with the thermal energy of clusters of similar dimensions, suggesting the possibility of a uniform distribution of the elements.^[61] In the present study, the absence of a Cu_2O shell on the surface, along with the greater atomic percentage of elemental Au ($\approx 88\%$) than that in the volume of AuCuNTs ($\approx 85\%$) suggests that Cu atoms migrate into the core of the AuCuNTs without any phase segregation (Statement 4).

The above four statements are based on experimental evidences. Building upon these and previous reports on the unique reactivity of low coordinated surface atoms of larger metallic NPs showing unique/specific reactions towards NCs,^[30,64,65] we propose a plausible reaction mechanism between AuNT and Cu_{18} NCs (**Scheme 1**):

- 1) Cu_{18} was decomposed into $[\text{Cu}_x\text{DPPE}_y]^+$ ($x = 1, y = 1, 2$) in the reaction medium.
- 2) These Cu-DPPE complexes first formed an adduct with the partially unprotected AuNT surface. Although could not be isolated in this case, such adducts are previously identified as intermediates of inter-AgNP-AuNC reaction,^[66] as well as AuNT-Ag₂₅ NC reaction.^[64]
- 3) Metal-DPPE bond being labile, DPPE moieties freely migrate between neighboring Au and Cu atoms at AuNT surface. As demonstrated by Peng et al.^[63] and Wang et al.,^[63] $[\text{Au}_2(\text{DPPE})_2]^{2+}$ moieties were eventually detached from the nanoparticle, Cu atoms taking up the space of Au atoms.
- 4) Finally, to reduce surface energy, Cu atoms migrated to the core making room for further reaction while keeping the morphology intact.

Motivated by their exceptional efficacy in plasmonic, catalytic, and biomedical applications, significant efforts have been made

to fabricate Au–Cu alloy NPs of diverse geometries.^[16] However, due to inherent disparities in lattice constants between Au and Cu, minor variations in experimental conditions can significantly alter the reaction kinetics and pathways, especially for complex shapes. Bimetallic phase formation can't be deduced from the intrinsic thermodynamic predictors, like reduction potentials. Rather, it depends on the reaction kinetics (i.e., side reactions) and constantly variable thermodynamics, including ligand exchange, making it complicated. Acknowledging the demand for a generic alloying strategy, we extended our protocol to synthesize Au–Cu alloy NPs of alternative shapes. Among various anisotropic structures, monodisperse cubes are of great interest as building blocks in designing novel hierarchical nanostructures suitable for devices.^[67,68] AuCuNCBs of a range of sizes have been synthesized using a one-pot polyol strategy, which still requires elevated temperature.^[20] On the other hand, AuNRs, characterized by their high-index surface facets,^[69] have been applied across a broad spectrum of fields. Chen et al. have reported that Au–Cu alloy nanorod catalysts show nearly twice the catalytic efficiency compared to their spherical counterparts despite possessing a 4-fold reduced total surface area.^[70] Synthetic procedures of high-quality AuNCBs and AuNRs are well documented in the literature. Here, AuNCBs with an approximate edge length of 50 nm and AuNRs with dimensions of roughly 30 nm (length) by 10 nm (width) were synthesized,^[71] and subsequently treated with Cu_{18} in a similar manner. According to Meena et al., CTAB forms a layer of distorted cylindrical micelles on AuNR surfaces.^[72] Channels among these micelles allow reactants to freely diffuse from the bulk solution to the gold surface facilitating a similar reaction as observed in the case of CTAC protected AuNTs. The resulting products were examined using UV–vis absorption spectra, TEM, and field emission scanning electron microscopy (FESEM) (characterization details are included in **Figure 3**; Figures S8, and S9, Supporting Information). TEM image of the resulting AuCuNCBs, shown in **Figure 3a**, confirms the preservation of monodispersity in size and shape, including edge sharpness. FESEM image of a single AuCuNCb is presented in **Figure 3b**. Spot EDS collected from the center of the particle reveals a composition of 36 atomic percent Cu and 64 atomic percent Au. Further, EDS line profiling (**Figure 3c**) along the yellow line shows a homogeneous distribution of Au and Cu within the reacted AuNCb. Similarly, **Figure 3d** presents a TEM image of AuCuNRs. FESEM image of them (**Figure 3e**), along with the simultaneously acquired line scan spectrum (**Figure 3f**), illustrates an even distribution of both metals along the nanostructure, with spot EDS analysis yielding $\approx 78\%$ Au and 22% Cu. These findings validate that interaction with Cu_{18} NC converts AuNPs of

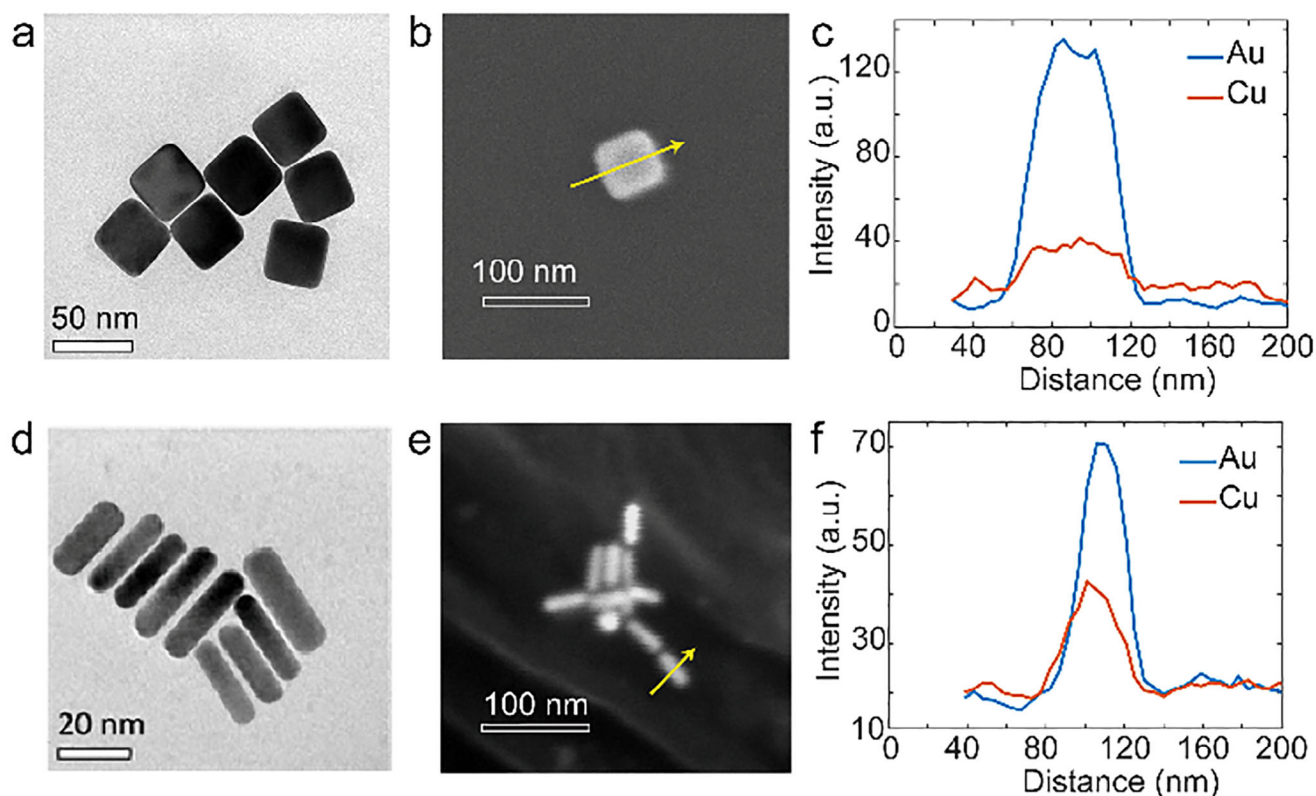


Figure 3. Au–Cu alloying in nanocubes and nanorods. a) TEM image of the AuCuNCBs, b) FESEM image of a single AuCuNCb with point EDS collected from the center, c) FESEM EDS line profile across the AuCuNCb particle along the yellow line, d) TEM image of the AuCuNRs, e) FESEM image of AuCuNRs, f) EDS line profile along the yellow line across the NR at the bottom.

any dimension and transforms them into Au–Cu alloy NPs while maintaining their original morphology, marking the first known shape-independent method for fabricating Au–Cu alloy NPs at room temperature, to the best of our knowledge.

We believe that the challenges associated with the fabrication of trimetallic NPs of desired non-spherical morphology may be overcome by using NCs as precursors. As proof of this concept, the solution-phase reactivity of Ag_{25} NC toward AuCuNTs was explored, and the resultant particles were subjected to comprehensive characterization. **Figure 4a** shows the dark-field STEM image of the NTs post-reaction. Noticeable blunting of the NTs at the tips and edges along with a reduction in edge length (Figure S10, Supporting Information) can be observed which indicates atomic etching at sites with low coordination. The bright-field STEM image of a single particle, along with the corresponding EDS line profile (in Figure 4b), reveals the homogeneous distribution of Au, Ag, and Cu along the NTs. The elemental STEM mapping of the particles, shown in Figure 4c, further supports the transformation of bimetallic AuCuNTs into trimetallic AuCuAgNTs following the interaction with Ag_{25} NC. However, the low atomic percentage of Ag (below 10%) within the AuCuAgNTs and the unaltered XRD peak positions, as compared to parent AuCuNTs (not shown), suggest that the doping of Ag was limited to the surface of the NTs, as opposed to complete alloying. These observations are consistent with the reactivity of Ag_{25} toward pure AuNTs^[29] and suggests that the reactivity of different Ag NCs with AuNTs can be extended to alloy AuCuNPs to

achieve diverse trimetallic NPs. Thus, our strategy shows the reproducibility and the robust nature of inter-nanoparticle reaction schemes, potentially encouraging the community to explore the reactivity of the other NCs to successfully tune the composition of nanostructures with intricate shapes.

3. Conclusion

In conclusion, we propose a novel strategy to fabricate alloy bimetallic NPs of targeted morphology by using anisotropic AuNPs as scaffolds through their reactivity with Cu_{18} NCs. Specifically, we demonstrated that Cu_{18} NCs serve as a precursor to incorporate Cu(0) into AuNTs, facilitating the formation of uniform AuCuNTs in DMF. This transformation fully conserves the size and shape of the parent nanostructure, occurs at room temperature, and requires no special equipment. The formation of alloys was confirmed from XRD analysis, while their composition was determined from electron microscopic elemental analyses, and ICP MS. Using AuNCBs and AuNRs, the general applicability of the protocol was proven. Finally, leveraging the reactivity of Ag_{25} toward AuCuNTs, trimetallic AuCuAg NTs were successfully synthesized. Thus, the methodology presented herein addresses the challenge of synthesizing multimetallic anisotropic NPs with high shape and size monodispersity. With the wide range of Au NPs and metallic NCs documented in scientific literature, the present study shows enormous potential

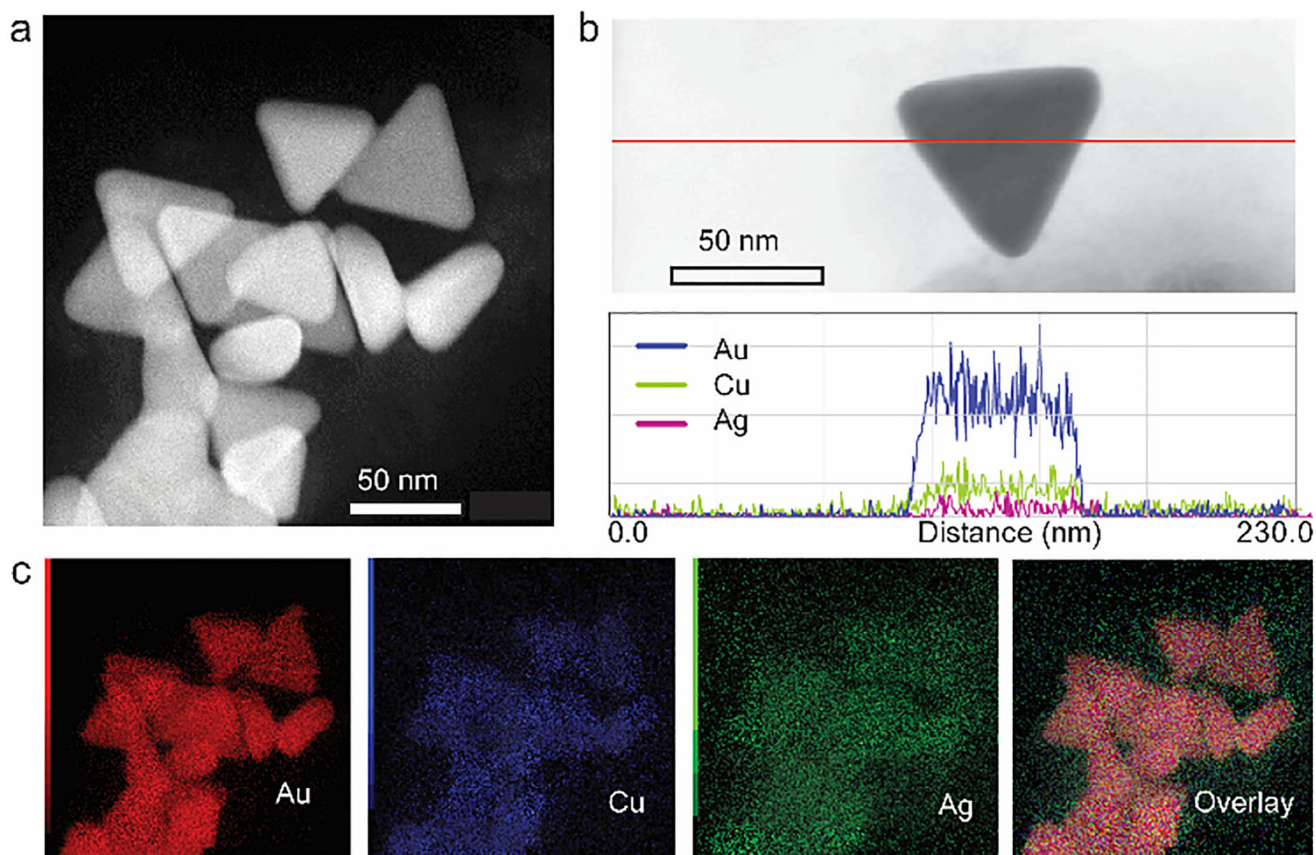


Figure 4. Characterization of AuCuAgNT. a) Dark-field STEM image of AuCuAgNTs, b) STEM EDS line profile of a single AuCuAgNT, c) STEM EDS elemental mapping corresponding to Figure a. Due to their random orientation on the TEM grid, some NTs appear as different shapes in their 2D projections.

in fabricating functional nanomaterials through the strategic selection of reactant pairs.

Supporting Information

Supporting Information is available from the Wiley Online Library or from the author.

Acknowledgements

A.C. and S.M. contributed equally to this work. The authors thank the Department of Science and Technology, the Government of India, and IIT Madras for supporting the research. A.C. and S.M., respectively, thank the Council of Scientific and Industrial Research and UGC for their research fellowships. The authors acknowledge the Research Council of Finland for project funding (No. 352900), Photonics Research and Innovation (PREIN) flagship, and Tampere Microscopy Centre for imaging facilities. T.P. thanks the Science and Engineering Research Board (SERB), India, for funding through the SPR/2021/000439 research grant, SUPRA project, and the JC Bose Fellowship. T.P. acknowledges funding from the Centre of Excellence (CoE) on Molecular Materials and Functions from the Institute of Eminence scheme of IIT Madras. A.C. was responsible for the conception and design of the work. A.C. and S.M. performed the experiments, analyzed the data, and prepared the manuscript. B.M. performed the transmission electron microscopy. M.B. helped with the synthesis of the nanoclusters. A.N. performed scanning electron microscopy. S.C. performed

the XPS, T.N. performed the ICP MS, and N. performed the scanning transmission electron microscopy. T.P. supervised the study and helped to improve the manuscript.

Conflict of Interest

The authors declare no conflict of interest.

Data Availability Statement

The data that support the findings of this study are available from the corresponding author upon reasonable request.

Keywords

alloy nanoparticles, copper nanoclusters, morphology-preserved alloying, noble metal nanoparticles, trimetallic nanoparticles

Received: November 15, 2024

Revised: April 3, 2025

Published online:

- [1] K. L. Kelly, E. Coronado, L. L. Zhao, G. C. Schatz, *J. Phys. Chem. B* **2003**, *107*, 668.
- [2] H. Wang, D. W. Brandl, P. Nordlander, N. J. Halas, *Acc. Chem. Res.* **2007**, *40*, 53.
- [3] Y. Wang, J. Chen, Y. Zhong, S. Jeong, R. Li, X. Ye, *J. Am. Chem. Soc.* **2022**, *144*, 13538.
- [4] J. Reguera, J. Langer, D. J. de Aberasturi, L. M. Liz-Marzán, *Chem. Soc. Rev.* **2017**, *46*, 3866.
- [5] C. L. Bracey, P. R. Ellis, G. J. Hutchings, *Chem. Soc. Rev.* **2009**, *38*, 2231.
- [6] D. D. Robertson, M. L. Personick, *Chem. Mater.* **2019**, *31*, 1121.
- [7] R. He, Y.-C. Wang, X. Wang, Z. Wang, G. Liu, W. Zhou, L. Wen, Q. Li, X. Wang, X. Chen, J. Zeng, J. G. Hou, *Nat. Commun.* **2014**, *5*, 4327.
- [8] E. C. Garnett, M. L. Brongersma, Y. Cui, M. D. McGehee, *Annu. Rev. Mater. Res.* **2011**, *41*, 269.
- [9] X. Liu, D. Wang, Y. Li, *Nano Today* **2012**, *7*, 448.
- [10] R. Borah, S. Verbruggen, *J. Phys. Chem. C* **2020**, *124*, 12081.
- [11] A. Loiseau, L. Zhang, D. Hu, M. Salmain, Y. Mazouzi, R. Flack, B. Liedberg, S. Boujday, *ACS Appl. Mater. Interfaces.* **2019**, *11*, 46462.
- [12] J.-H. Lee, G.-H. Kim, J.-M. Nam, *J. Am. Chem. Soc.* **2012**, *134*, 5456.
- [13] Y. Xia, K. D. Gilroy, H.-C. Peng, X. Xia, *Angew. Chem., Int. Ed.* **2017**, *56*, 60.
- [14] Z. D. Pozun, S. E. Rodenbusch, E. Keller, K. Tran, W. Tang, K. J. Stevenson, G. Henkelman, *J. Phys. Chem. C* **2013**, *117*, 7598.
- [15] Z. Wang, Y. Ju, S. Tong, H. Zhang, J. Lin, B. Wang, Y. Hou, *Nanoscale Horiz.* **2018**, *3*, 624.
- [16] S. Thota, S. Chen, J. Zhao, *Chem. Commun.* **2016**, *52*, 5593.
- [17] A. Ngamaroonchote, Y. Sanguansap, T. Wutikhun, K. Karn-orachai, *Microchim. Acta* **2020**, *187*, 559.
- [18] A. K. Bentley, S. E. Skrabalak, *J. Chem. Educ.* **2023**, *100*, 3425.
- [19] H. Jung, M. E. King, M. L. Personick, *Curr. Opin. Colloid Interface Sci.* **2019**, *40*, 104.
- [20] Y. Liu, A. R. H. Walker, *Angew. Chem., Int. Ed.* **2010**, *49*, 6781.
- [21] A. Henkel, A. Jakob, G. Brunklau, C. Sönnichsen, *J. Phys. Chem. C* **2009**, *113*, 2200.
- [22] M. Hajfathalian, K. D. Gilroy, A. Yaghoobzade, A. Sundar, T. Tan, R. A. Hughes, S. Neretina, *J. Phys. Chem. C* **2015**, *119*, 17308.
- [23] I. Chakraborty, T. Pradeep, *Chem. Rev.* **2017**, *117*, 8208.
- [24] T. Pradeep, *Atomically Precise Metal Nanoclusters*, Elsevier, Amsterdam, Netherlands **2022**.
- [25] S. Nematulloev, A. Sagadevan, B. Alamer, A. Shkurenko, R. Huang, J. Yin, C. Dong, P. Yuan, K. E. Yorov, A. A. Karluk, W. J. Mir, B. E. Hasanov, M. Nejib Hedhili, N. M. Halappa, M. Eddaoudi, O. F. Mohammed, M. Rueping, O. M. Bakr, *Angew. Chem., Int. Ed.* **2023**, *62*, 202303572.
- [26] A. Som, I. Chakraborty, T. A. Maark, S. Bhat, T. Pradeep, *Adv. Mater.* **2016**, *28*, 2827.
- [27] A. Chakraborty, A. C. Fernandez, A. Som, B. Mondal, G. Natarajan, G. Paramasivam, T. Lahtinen, H. Häkkinen, T. P. Nonappa, *Angew. Chem., Int. Ed.* **2018**, *57*, 6522.
- [28] K. R. Krishnadas, A. Ghosh, A. Baksi, I. Chakraborty, G. Natarajan, T. Pradeep, *J. Am. Chem. Soc.* **2016**, *138*, 140.
- [29] A. Chakraborty, M. M. Stanley, B. Mondal, Nonappa, M. B., P. Chakraborty, M. P. Kannan, T. Pradeep, *Nanoscale* **2023**, *15*, 2690.
- [30] P. Bose, J. Roy, V. Khokhar, B. Mondal, G. Natarajan, S. Manna, V. Yadav, A. Nyayban, S. S. R. K. C. Yamijala, T. P. Nonappa, *Chem. Mater.* **2024**, *36*, 7581.
- [31] J. Li, H. Z. Ma, G. E. Reid, A. J. Edwards, Y. Hong, J. M. White, R. J. Mulder, R. A. J. O'Hair, *Chem. – Eur. J.* **2018**, *24*, 2070.
- [32] L. Scarabelli, M. Coronado-Puchau, J. J. Giner-Casares, J. Langer, L. M. Liz-Marzán, *ACS Nano* **2014**, *8*, 5833.
- [33] D. Kim, J. Resasco, Y. Yu, A. M. Asiri, P. Yang, *Nat. Commun.* **2014**, *5*, 4948.
- [34] Z. Niu, S. Chen, Y. Yu, T. Lei, A. Dehestani, K. Schierle-Arndt, P. Yang, *Nano Res.* **2020**, *13*, 2564.
- [35] S. Alayoglu, P. Zavalij, B. Eichhorn, Q. Wang, A. I. Frenkel, P. Chupas, *ACS Nano* **2009**, *3*, 3127.
- [36] G. Yang, D. Chen, P. Lv, X. Kong, Y. Sun, Z. Wang, Z. Yuan, H. Liu, J. Yang, *Sci. Rep.* **2016**, *6*, 35252.
- [37] F. Chang, C. Wang, X. Wu, Y. Liu, J. Wei, Z. Bai, L. Yang, *Materials* **2022**, *15*, 5064.
- [38] A. K. Sra, T. D. Ewers, R. E. Schaak, *Chem. Mater.* **2005**, *17*, 758.
- [39] C. M. Andolina, A. C. Dewar, A. M. Smith, L. E. Marbella, M. J. Hartmann, J. E. Millstone, *J. Am. Chem. Soc.* **2013**, *135*, 5266.
- [40] S. Dai, T.-H. Huang, W.-I. Liu, C.-W. Hsu, S.-W. Lee, T.-Y. Chen, Y.-C. Wang, J.-H. Wang, K.-W. Wang, *Nano Lett.* **2021**, *21*, 9293.
- [41] X. Ye, X. He, Y. Lei, J. Tang, Y. Yu, H. Shi, K. Wang, *Chem. Commun.* **2019**, *55*, 2321.
- [42] X. T. Van, L. T. Trinh, H. Van Pham, M. T. T. Nguyen, *J. Electron. Mater.* **2022**, *51*, 1857.
- [43] B. Shan, Y. Zhao, Y. Li, H. Wang, R. Chen, M. Li, *Chem. Mater.* **2019**, *31*, 9875.
- [44] M. B. Gawande, A. Goswami, F.-X. Felpin, T. Asefa, X. Huang, R. Silva, X. Zou, R. Zboril, R. S. Varma, *Chem. Rev.* **2016**, *116*, 3722.
- [45] Y. Wang, X. Duan, J. Zheng, H. Lin, Y. Yuan, H. Ariga, S. Takakusagi, K. Asakura, *Catal. Sci. Technol.* **2012**, *2*, 1637.
- [46] L. Chen, Y. Zhang, P. Zhu, F. Zhou, W. Zeng, D. D. Lu, R. Sun, C. Wong, *Sci. Rep.* **2015**, *5*, 9672.
- [47] A. Sakthisabarimoorathi, M. Jose, S. A. Martin Britto Dhas, S. J. Das, *J. Mater. Sci. Mater. Electron.* **2017**, *28*, 4545.
- [48] M. C. Biesinger, *Surf. Interface Anal.* **2017**, *49*, 1325.
- [49] S. Alayoglu, P. Zavalij, B. Eichhorn, Q. Wang, A. I. Frenkel, P. Chupas, *ACS Nano* **2009**, *3*, 3127.
- [50] W. J. Plieth, *Surf. Sci.* **1985**, *156*, 530.
- [51] Z. Wu, *Angew. Chem.* **2012**, *124*, 2988.
- [52] Z. Gan, N. Xia, Z. Wu, *Acc. Chem. Res.* **2018**, *51*, 2774.
- [53] M. Wang, Z. Wu, Z. Chu, J. Yang, C. Yao, *Chem. – Asian J.* **2014**, *9*, 1006.
- [54] S. Tian, C. Yao, L. Liao, N. Xia, Z. Wu, *Chem. Commun.* **2015**, *51*, 11773.
- [55] Z. Wu, M. Wang, J. Yang, X. Zheng, W. Cai, G. Meng, H. Qian, H. Wang, R. Jin, *Small* **2012**, *8*, 2027.
- [56] M. Zhu, P. Wang, N. Yan, X. Chai, L. He, Y. Zhao, N. Xia, C. Yao, J. Li, H. Deng, Y. Zhu, Y. Pei, Z. Wu, *Angew. Chem., Int. Ed.* **2018**, *57*, 4500.
- [57] C. Yao, J. Chen, M.-B. Li, L. Liu, J. Yang, Z. Wu, *Nano Lett.* **2015**, *15*, 1281.
- [58] R. Ciganda, N. Li, C. Deraedt, S. Gatard, P. Zhao, L. Salmon, R. Hernández, J. Ruiz, D. Astruc, *Chem. Commun.* **2014**, *50*, 10126.
- [59] S. K. Meena, S. Celiksoy, P. Schäfer, A. Henkel, C. Sönnichsen, M. Sulpizi, *Phys. Chem. Chem. Phys.* **2016**, *18*, 13246.
- [60] J. Peng, B. Huang, P. Wang, Y. Pei, *J. Phys. Chem. A* **2022**, *126*, 8910.
- [61] G. Guisbiers, S. Mejia-Rosales, S. Khanal, F. Ruiz-Zepeda, R. L. Whetten, M. José-Yacamán, *Nano Lett.* **2014**, *14*, 6718.
- [62] S. Jeong, Y. Liu, Y. Zhong, X. Zhan, Y. Li, Y. Wang, P. M. Cha, J. Chen, X. Ye, *Nano Lett.* **2020**, *20*, 7263.
- [63] S. Wang, H. Abroshan, C. Liu, T.-Y. Luo, M. Zhu, H. J. Kim, N. L. Rosi, R. Jin, *Nat. Commun.* **2017**, *8*, 848.
- [64] A. Chakraborty, M. M. Stanley, B. Mondal, Nonappa, M. B., P. Chakraborty, M. P. Kannan, T. Pradeep, *Nanoscale* **2023**, *15*, 2690.
- [65] A. Som, A. K. Samal, T. Udayabhaskararao, M. S. Bootharaju, T. Pradeep, *Chem. Mater.* **2014**, *26*, 3049.
- [66] P. Bose, P. Chakraborty, J. S. Mohanty, Nonappa, A. R. C., E. Khatun, T. Ahuja, A. Mahendranath, T. Pradeep, *Nanoscale* **2020**, *12*, 22116.
- [67] B. Gao, G. Arya, A. R. Tao, *Nat. Nanotechnol.* **2012**, *7*, 433.

- [68] G. Singh, H. Chan, A. Baskin, E. Gelman, N. Repnin, P. Král, R. Klajn, *Science* **2014**, *345*, 1149.
- [69] E. Carbó-Argibay, B. Rodríguez-González, S. Gómez-Graña, A. Guerrero-Martínez, I. Pastoriza-Santos, J. Pérez-Juste, L. M. Liz-Marzán, *Angew. Chem., Int. Ed.* **2010**, *49*, 9397.
- [70] S. Chen, S. V. Jenkins, J. Tao, Y. Zhu, J. Chen, *J. Phys. Chem. C* **2013**, *117*, 8924.
- [71] A. K. Samal, T. S. Sreepasad, T. Pradeep, *J. Nanoparticle Res.* **2010**, *12*, 1777.
- [72] S. K. Meena, M. Sulpizi, *Langmuir* **2013**, *29*, 14954.